



**Nuclearity Effects in Supported, Single-Site Fe(II)
Hydrogenation Pre-Catalysts**

Journal:	<i>Dalton Transactions</i>
Manuscript ID	DT-COM-07-2018-002720
Article Type:	Communication
Date Submitted by the Author:	03-Jul-2018
Complete List of Authors:	<p>Langeslay, Ryan R.; Argonne National Laboratory, Chemical Sciences and Engineering Division Sohn, Hyuntae; Argonne National Laboratory Mohar, Jacob; Michigan Technological University, chemistry Hu, Bo; Illinois Institute of Technology, Biological and Chemical Sciences Ferrandon, Magali; Argonne National Laboratory, Chemical Sciences and Engineering Division Liu, Cong; Argonne National Laboratory, Chemical Sciences and Engineering Division Kim, Hacksung; Northwestern University, Department of Chemistry Kropf, A.; Argonne National Laboratory, Chemical Sciences and Engineering Division Yang, Ce; Argonne National Laboratory, Chemical Science and Engineering Niklas, Jens; Argonne National Laboratory, Chemical Sciences & Engineering Poluektov, Oleg; Argonne National Laboratory, Chemical Sciences and Engineering Division Alp, Ercan; Argonne National Laboratory, Advanced Photon Source Ignacio-de Leon, Patricia A. A.; Argonne National Laboratory, Energy Systems Division Sattelberger, Alfred; Argonne National Laboratory, Office of the Director Hock, Adam; Illinois Institute of Technology, Biological and Chemical Sciences Delferro, Massimiliano; Argonne National Laboratory, Chemical Sciences and Engineering Division</p>



Dalton Transactions

COMMUNICATION

Nuclearity Effects in Supported, Single-Site Fe(II) Hydrogenation Pre-Catalysts

Received 00th January 20xx,
Accepted 00th January 20xx

DOI: 10.1039/x0xx00000x

www.rsc.org/

Ryan R. Langeslay,^{a*} Hyuntae Sohn,^a Bo Hu,^{a,b} Jacob S. Mohar,^a Magali Ferrandon,^a Cong Liu,^a Hacksung Kim,^{a,c} A. Jeremy Kropf,^a Ce Yang,^a Jens Niklas,^a Oleg G. Poluektov,^a E. Ercan Alp,^d Patricia Ignacio-de Leon,^e Alfred P. Sattelberger,^{a*} Adam S. Hock^{a,b*} and Massimiliano Delferro^{a*}

Dimeric and monomeric supported single-site Fe(II) pre-catalysts on SiO₂ have been prepared via organometallic grafting and characterized with advanced spectroscopic techniques. Manipulation of the surface hydroxyl concentration on the support influences monomer/dimer formation. While both pre-catalysts are highly active in liquid-phase hydrogenation, the dimeric pre-catalyst is ~3x faster than the monomer. Preliminary XAS experiments on the H₂-activated samples suggest the active species are isolated Fe(II) sites.

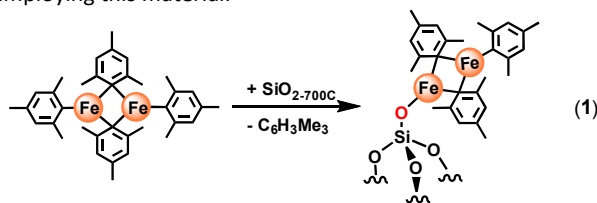
The need for chemicals throughout the world has increased the need for catalysts that perform desired chemical transformations with high efficiency. Catalysts that effect the hydrogenation of unsaturated bonds are one of the most critical types as these compounds have applications in the energy, pharmaceutical, agrochemical, and commodity chemical industries. As these industries grow and the demand for catalysts increases, the need to move away from precious metal catalysts toward more sustainable and cost-effective earth-abundant catalysts¹ such as those which contain first-row transition metals (Co,² Fe,² V³), has become an increasingly important endeavor.

In addition to employing first-row transition metals for catalysis, our lab and others⁴⁻¹⁰ are interested in utilizing Surface Organometallic Chemistry (SOMC)¹¹⁻¹⁵ to functionalize solid supports such as SiO₂, Al₂O₃, TiO₂ and ZrO₂. The combination of a tailored support surface and organic ancillary ligands can not only stabilize the metal coordination sphere through sterics, but also tune the electronic properties of the metal active site, which in turn may modulate the catalytic activity. Furthermore, catalytic function is likely influenced by metal nuclearity on the surface. As such, we are interested in

methods for manipulating and controlling the nuclearity and understanding how the imparted structures affect the catalytic performance.^{4, 7, 16} In addition, we are interested in understanding the influence and fate of the precursor ligands, as well as their role in catalytic processes.

Recently, it has been shown that Fe(II) single-atom¹⁷ ions supported on silica are active for propane dehydrogenation at 650 °C¹⁸ as well as methane aromatization at higher temperatures.¹⁹ In addition, homogeneous^{2, 20-22} and heterogeneous^{1, 23} iron catalysts are active in hydrogenation reactions. Furthermore, iron catalysts are found in enzymes such as methane monooxygenase,²⁴ which contains a bimetallic iron core, and the FeMo cofactor of nitrogenase,²⁵ which is a cluster containing multiple iron centers. These multimetallic systems are able to catalyze reactions in ways that monometallic systems cannot. As such, chemists have long sought to understand the fundamental chemistry of these cooperative catalytic processes and to apply the knowledge to the rational design of new catalysts.

With this in mind, we decided to target dinuclear iron(II) complexes as molecular precursors to generate supported single-site iron(II) catalysts for alkene hydrogenation. This approach offered several avenues for gaining insight such as understanding how the surface structure affects metal nuclearity and whether or not the resulting nuclearity can induce metal-metal cooperative effects.^{26, 27} An intriguing report by Copéret and coworkers proposed the bimetallic precursor [Fe(μ-Mes)Mes]₂²⁸ (Mes = C₆H₂(CH₃)₃) reacts with SiO₂ dehydroxylated at 700 °C (SiO₂₋₇₀₀) to form a likely terminally-bound surface bimetallic species according to eqn 1.²⁹ However, no catalytic tests have been reported to date employing this material.



It is known that the hydroxyl concentration on the surface of amorphous silica is tunable and various degrees of dehydroxylation can be achieved by thermal treatment.^{13, 30} As

^a Chemical Sciences and Engineering Division, Argonne National Laboratory, Lemont, IL 60439, USA. E-mail: lanqesrr@anl.gov, asattelberger@anl.gov, delferro@anl.gov

^b Department of Chemistry, Illinois Institute of Technology, Chicago IL 60616, USA. E-mail: ahock@iit.edu

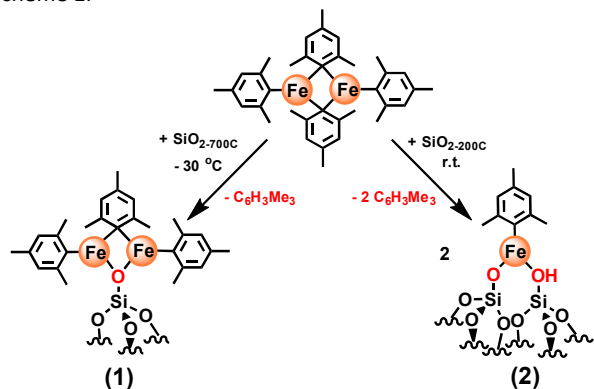
^c Catalysis Center, Northwestern University, Evanston, IL 60208, USA

^d X-ray Science Division, Argonne National Laboratory, Lemont, IL 60439, USA

^e Energy Sciences Division, Argonne National Laboratory, Lemont, IL 60439, USA
Electronic Supplementary Information (ESI) available: See DOI: 10.1039/x0xx00000x

a consequence, it may be possible to affect the surface species by varying the support surface in this way. Two silica supports, SiO_{2-700} and SiO_{2-200} , were prepared by heating the same batch of silica gel to 700 °C and 200 °C, respectively, under vacuum (15 mtorr) for 12 h, resulting in partially-dehydroxylated silica with silanol concentrations of ca. 0.8^{13} and 4.9^3 OH/nm², respectively. Diffuse Reflectance Infrared Fourier Transform Spectroscopy (DRIFTS) shows a decrease in the vicinal silanols in SiO_{2-700} compared to SiO_{2-200} as seen by the loss of the broad signal centred around 3500 cm⁻¹ (Figure S1). The result is that SiO_{2-700} contains mostly isolated silanols (5-10% geminal¹³), while SiO_{2-200} contains a larger number of vicinal silanols.

The dimeric precursor $[\text{Fe}(\mu\text{-Mes})\text{Mes}]_2$ reacts with SiO_{2-700} in toluene at -30 °C to form the air-sensitive reddish-brown bimetallic FeSiO_{2-700} (**1**), Scheme 1. It will be seen that, through a combination of spectroscopic techniques, the structure of **1** is different from that previously proposed (*vide infra*). In addition, a green, air-sensitive, monometallic analogue, FeSiO_{2-200} (**2**) can be generated by reacting the same precursor, $[\text{Fe}(\mu\text{-Mes})\text{Mes}]_2$, with SiO_{2-200} in toluene at room temperature, Scheme 1.



Scheme 1. Synthesis of FeSiO_{2-700} , **1**, and FeSiO_{2-200} , **2**.

NMR grafting experiments show that, during the synthesis of **1**, one mole of mesitylene is liberated per mole $[\text{Fe}(\mu\text{-Mes})\text{Mes}]_2$, and during the synthesis of **2**, ca. 2.1 moles are liberated per mole $[\text{Fe}(\mu\text{-Mes})\text{Mes}]_2$, Figure S2. Elemental analysis was conducted on compounds **1** and **2** and these data are consistent with the grafting studies. For **1**, the surface iron concentration was 1.73% with a carbon-to-iron ratio of 3.25, in reasonable agreement with the calculated value of 2.9 for a $[\text{Fe}_2(\text{Mes})_3]$ unit. For **2**, the surface iron concentration was 1.52% and a carbon-to-iron ratio of ca. 1.6 was found corresponding to 0.8 mesityl ligands per iron center.

EPR spectroscopy was used to probe the oxidation states after grafting (Figures S3-S6). Both **1** and **2** show high-spin Fe(II) signals, in agreement with XANES analysis (Figure S13). Upon exposure to air, both compounds rapidly oxidize to Fe(III). Compounds **1** and **2** were characterized by DRIFTS, Figure S7. The spectra of **1** and **2** exhibit bands at 2800-3100 cm⁻¹ and 1600 cm⁻¹ corresponding to the C-H and C=C modes of the mesitylene ligands, respectively, suggesting the presence of an organo-iron fragment on the SiO_2 supports. The Diffuse Reflectance Ultraviolet-Visible (DRUV) spectra of **1**, **2**, and $[\text{Fe}(\mu\text{-Mes})\text{Mes}]_2$ show the electronic similarity between **1** and $[\text{Fe}(\mu\text{-Mes})\text{Mes}]_2$, Figure S8. All three compounds absorb over a broad range of wavelengths in the visible region and contain a major feature at high energy (λ_{max} at 375, 360, and 410 nm for **1**, **2**,

and $[\text{Fe}(\mu\text{-Mes})\text{Mes}]_2$, respectively). However, compounds **1** and $[\text{Fe}(\mu\text{-Mes})\text{Mes}]_2$ also contain a second broad feature at 495 and 525 nm, respectively, which is not observed in **2**. This common feature at lower energy suggests a similar geometry between **1** and $[\text{Fe}(\mu\text{-Mes})\text{Mes}]_2$, which is consistent with the identification of **1** as the surface structure (see Figure S9 for visual color comparison).

The surface structures of **1** and **2** were probed by Raman spectroscopy in order to identify the presence or absence of bridging mesityl ligands, which would inform on the dimeric or monomeric nature of the surface sites, respectively. A comparison of **1** and **2** with their respective silica supports, the $[\text{Fe}(\mu\text{-Mes})\text{Mes}]_2$ precursor, and free mesitylene, is shown in Figure 1. Density Functional Theory (DFT) was used to assign the bands in the spectra. A comparison of the experimental vibrational frequencies with those computed from the optimized surface structures (*vide infra*) is reported in Table S1. The bands centered around 560 cm⁻¹, which are only present in $[\text{Fe}(\mu\text{-Mes})\text{Mes}]_2$ and **1**, are assigned to the Fe-C-Fe stretching vibrations. This matches well with the calculated value of 550 cm⁻¹, confirming the dimeric nature of iron in **1**.

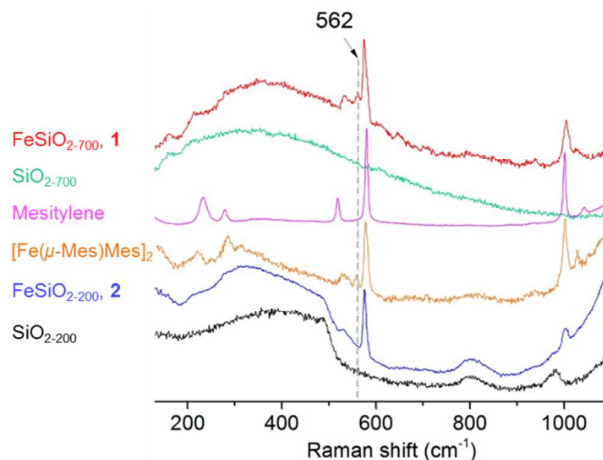


Figure 1. Raman spectra of **1** (red), SiO_{2-700} (teal), mesitylene (pink), $[\text{Fe}(\mu\text{-Mes})\text{Mes}]_2$ (orange), **2** (blue) and SiO_{2-200} (black)

The presence of iron in **1** and **2** allowed investigation by Mössbauer spectroscopy, and their respective spectra are shown in Figure 2. The spectrum of compound **1** indicates the presence of only one unique iron center with $\delta = 0.96$ mm/s and $\Delta E_Q = 1.91$ mm/s, favoring the (μ -oxo) structure shown for **1** in Scheme 1 over the terminally-bound structure previously proposed²⁹ and shown in eqn 1. The terminally-bound structure should have two distinct iron signals, stemming from the two unique iron environments (i.e., an asymmetric molecule). While the (μ -oxo) structure was originally disfavored due to the higher reactivity of terminal vs bridging ligands, it is not unreasonable to imagine an initial reaction to form the terminally-bound structure which then rearranges to the (μ -oxo) structure. Analysis of the spectrum of **2** indicates a mixture of species, with the major component (92%) having $\delta = 0.56$ mm/s and $\Delta E_Q = 1.02$ mm/s, and the minor component having $\delta = 0.65$ mm/s and $\Delta E_Q = 2.17$ mm/s. This minor component may be a thermal degradation product or a surface iron that does not contain a mesitylene ligand. The ferric product produced when **2** is exposed to air has a smaller isomer shift and quadrupole splitting of 0.25 mm/s and 0.92 mm/s, respectively, Figure 2.

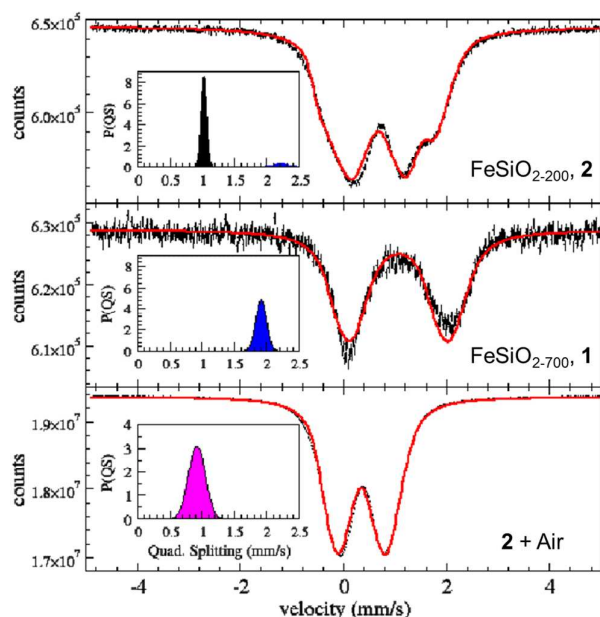


Figure 2. Mössbauer spectra of **2** (top), **1** (middle), and **2** after air exposure (bottom). The inserts represent the probability distribution function of the sample quadrupole splitting values.

DFT calculations were carried out to study the surface structures of **1** and **2** using cluster models for the silica support.³³ For **1**, both the terminally-bound and (μ -oxo) structures were considered, but only the (μ -oxo) structure converged from the calculations, Figure 3. The 2.76 Å Fe-Fe distance in the optimized (μ -oxo) structure of **1** is slightly longer than the 2.62 Å distance in $[\text{Fe}(\mu\text{-Mes})\text{Mes}]_2$.²⁸ For **2**, both 3- and 4-coordinate Fe structures were found (Figure S11), with the 4-coordinate (Figure 3) being more stable by 2.2 kcal/mol.

Pre-catalysts **1** and **2** were found to be active catalysts for the hydrogenation of olefins at 25 °C in the presence of H_2 . The reaction of **1** and **2** with H_2 presumably forms surface iron hydride species, which are known to affect hydrogenation reactions,³⁴ and specific homogeneous examples with iron are in the literature.³⁵⁻³⁷ Hydrogenation reactions were conducted with liquid substrates in batch reactors. First, the hydrogenation of cyclohexene was examined. Since the hydrogenation of cyclohexene can only yield one product, cyclohexane, H_2 gas consumption was used to measure the kinetics. Under the same catalytic conditions (100 mg catalyst, 200 psi H_2 , 0.25 M cyclohexene in dodecane, 700 rpm, 25 °C), pre-catalysts **1** and **2** react with initial turnover frequencies (TOFs) of 0.082 and 0.027 s^{-1} , respectively, Figure 4. Interestingly, the initial TOF of **1** is ~ 3 x faster than that of **2**.

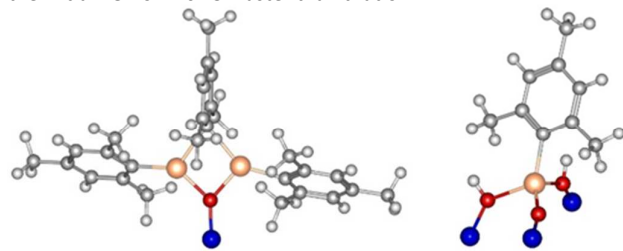


Figure 3. DFT calculated (B3LYP/CEP-31G) structures of **1** (left) and **2** (right). The SiO_2 cluster has been omitted for clarity. C, gray; Fe,

orange; O, red; Si, blue. Full models including SiO_2 clusters are shown in Figures S10 and S11.

The hydrogenation of 1-octene was also attempted in order to confirm the generality of the difference in reactivity observed between **1** and **2**. Both pre-catalysts **1** and **2** rapidly hydrogenate 1-octene (50 mg pre-catalyst, 200 psi H_2 , 0.25 M 1-octene in dodecane, 700 rpm, 25 °C) to octane and internal olefins with initial rates of conversion to all products of $1.2(2) \times 10^{-4}$ M/s and $4.1(2) \times 10^{-5}$ M/s, respectively, Figure 4. Again it is observed that pre-catalyst **1** reacts ~ 3 x faster than **2**. Note that the internal olefins generated are then further hydrogenated to octane in these systems.

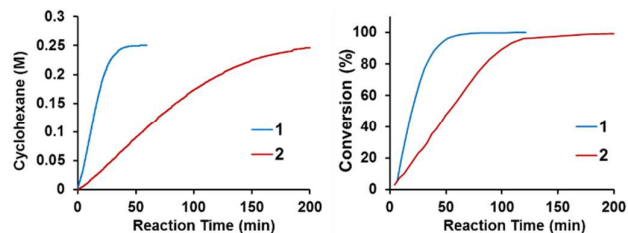


Figure 4. Hydrogenation results for **1** (blue) and **2** (red) for reactions with cyclohexene (left), and 1-octene (right).

Under these conditions, the reduction of isolated iron(II) species to iron(0) nanoparticles might occur. It has been shown that iron(0) nanoparticles are competent catalysts for the hydrogenation of alkenes.³⁸ However, the reaction conditions employed in this study (200 psi H_2 , 25 °C) are milder than those used to generate iron(0) nanoparticles (150 psi H_2 , 150 °C, 12 h).³⁸ In addition, the lack of induction period during catalysis suggests that the structure of the active species does not change over the course of the reaction. Nevertheless, TEM images were obtained on **1** and **2** as-prepared as well as after treatment with H_2 at 180 °C for 30 min, Figure S12, suggesting no apparent nanoparticle formation.³⁹ In addition, XAFS measurements indicate no iron metal nanoparticles for any of the samples, Figures S13 and S14. Defining quantitative sensitivity to metallic nanoparticles is difficult due to particle size effects. Nevertheless, the measurements strongly suggest no more than 5% of the Fe could be metallic. These data indicate that the iron(II) sites remain isolated even under reducing conditions at temperatures well above the hydrogenation reaction conditions.

Both **1** and **2** are extremely sensitive to oxygen and moisture. Samples oxidized to iron(III) by exposure to air rapidly darken in color and become inactive for hydrogenation, indicating iron(II) is the active species. The oxygen and moisture sensitivity has led to difficulties with reproducibility in the initial testing of gas-phase hydrogenation reactions. In addition, preliminary data indicate that thermal catalyst decomposition to inactive iron(II) species may also be operative in some cases as catalytic rates tend to decrease with pre-catalyst age.

In summary, modification of the degree of hydroxylation on the SiO_2 surface has allowed for the isolation and characterization of both dimeric and monomeric SiO_2 -supported iron(II) species generated from the same organometallic precursor. Both compounds can be activated with H_2 to form highly active hydrogenation catalysts, with the dimeric **1** forming an active catalyst having activity approximately 3x greater than that generated from the monomeric **2**. The higher activity of pre-catalyst **1** is likely due to nuclearity effects imposed by the SiO_2 surface

manipulation prior to grafting. Elucidation of the active species and mechanistic pathways will inform on the nature of the differences observed in these two catalysts. Structural characterization of the active species on silica, mechanistic studies, and decomposition/deactivation pathway investigations, through both experimental and computational avenues, are currently underway.

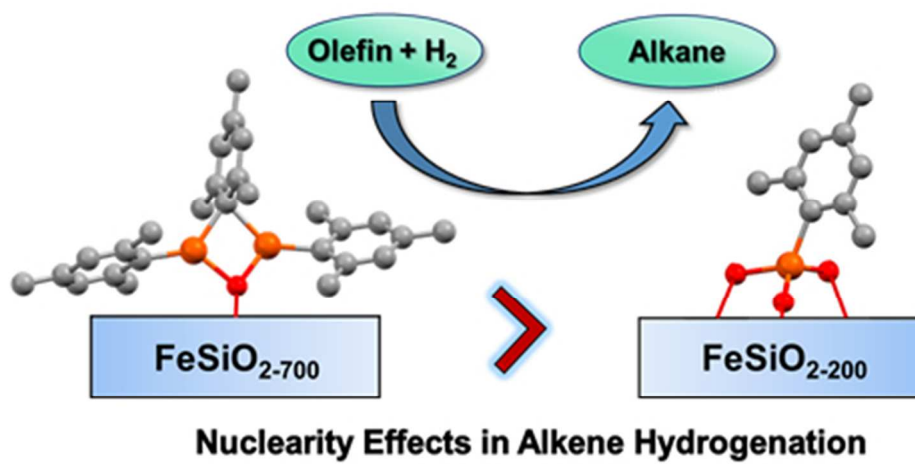
This work was supported by the U.S. Department of Energy, Office of Basic Energy Sciences, Division of Chemical Sciences, Geosciences, and Biosciences, under Contract DE-AC02-06CH11357 (Argonne National Laboratory). Use of the Advanced Photon Source is supported by the U.S. Department of Energy, Office of Science, and Office of Basic Energy Sciences, under Contract DE-AC02-06CH11357. MRCAT operations are supported by the Department of Energy and the MRCAT member institutions. DFT calculations were performed using the computational resources at the Argonne National Laboratory (ANL), Center for Nanoscale Materials (CNM) and resources provided by the Laboratory Computing Resource Center (LCRC) at ANL. Advanced Photon Source, a U.S. Department of Energy, Office of Science User Facility operated for the U.S. Department of Energy Office of Science by Argonne National Laboratory under Contract No. DE-AC02-06CH11357. H. K. acknowledges Dr. Emily Carino for the use of the Raman microscope.

Conflicts of interest

There are no conflicts to declare.

Notes and references

- D. Wang and D. Astruc, *Chem. Soc. Rev.*, 2017, **46**, 816-854.
- P. J. Chirik, *Acc. Chem. Res.*, 2015, **48**, 1687-1695.
- H. Sohn, J. Camacho-Bunquin, R. R. Langeslay, P. A. Ignacio-de Leon, J. Niklas, O. G. Poluektov, C. Liu, J. G. Connell, D. Yang, J. Kropf, H. Kim, P. C. Stair, M. Ferrandon and M. Delferro, *Chem. Commun.*, 2017, **53**, 7325-7328.
- A. W. Cook, Z. R. Jones, G. Wu, S. L. Scott and T. W. Hayton, *J. Am. Chem. Soc.*, 2018, **140**, 394-400.
- C. Copéret, A. Fedorov and P. A. Zhizhko, *Catal. Lett.*, 2017, **147**, 2247-2259.
- H. Tafazolian, D. B. Culver and M. P. Conley, *Organometallics*, 2017, **36**, 2385-2388.
- E. Guan and B. C. Gates, *ACS Catal.*, 2018, **8**, 482-487.
- M. M. Stalzer, C. P. Nicholas, A. Bhattacharyya, A. Motta, M. Delferro and T. J. Marks, *Angew. Chem. Int. Ed.*, 2016, **55**, 5263-5267.
- W. Gu, M. M. Stalzer, C. P. Nicholas, A. Bhattacharyya, A. Motta, J. R. Gallagher, G. Zhang, J. T. Miller, T. Kobayashi, M. Pruski, M. Delferro and T. J. Marks, *J. Am. Chem. Soc.*, 2015, **137**, 6770-6780.
- K. C. Szeto, A. Gallo, S. Hernández-Morejudo, U. Olsbye, A. De Mallmann, F. Lefebvre, R. M. Gauvin, L. Delevoye, S. L. Scott and M. Taoufik, *J. Phys. Chem. C*, 2015, **119**, 26611-26619.
- J. M. Basset, J. P. Candy and C. Copéret, in *Comprehensive Organometallic Chemistry III*, ed. R. H. Crabtree, Elsevier, Oxford, 2007, DOI: <https://doi.org/10.1016/B0-08-045047-4/00175-8>, pp. 499-553.
- C. Copéret, M. Chabanas, R. P. Saint-Arroman and J. M. Basset, *Angew. Chem. Int. Ed.*, 2003, **42**, 156-181.
- C. Copéret, A. Comas-Vives, M. P. Conley, D. P. Estes, A. Fedorov, V. Mougél, H. Nagae, F. Núñez-Zarur and P. A. Zhizhko, *Chem. Rev.*, 2016, **116**, 323-421.
- J. D. A. Pelletier and J.-M. Basset, *Acc. Chem. Res.*, 2016, **49**, 664-677.
- T. J. Marks, *Acc. Chem. Res.*, 1992, **25**, 57-65.
- M. K. Karunananda and N. P. Mankad, *ACS Catal.*, 2017, **7**, 6110-6119.
- J. Liu, *ACS Catal.*, 2017, **7**, 34-59.
- B. Hu, N. M. Schweitzer, G. Zhang, S. J. Kraft, D. J. Childers, M. P. Lanci, J. T. Miller and A. S. Hock, *ACS Catal.*, 2015, **5**, 3494-3503.
- X. Guo, G. Fang, G. Li, H. Ma, H. Fan, L. Yu, C. Ma, X. Wu, D. Deng, M. Wei, D. Tan, R. Si, S. Zhang, J. Li, L. Sun, Z. Tang, X. Pan and X. Bao, *Science*, 2014, **344**, 616-619.
- R. P. Yu, J. M. Darmon, J. M. Hoyt, G. W. Margulieux, Z. R. Turner and P. J. Chirik, *ACS Catal.*, 2012, **2**, 1760-1764.
- S. Enthaler, K. Junge and M. Beller, *Angew. Chem. Int. Ed.*, 2008, **47**, 3317-3321.
- J. C. Ott, C. K. Blasius, H. Wadepohl and L. H. Gade, *Inorg. Chem.*, 2018, DOI: 10.1021/acs.inorgchem.7b03227.
- N. C. Thacker, Z. Lin, T. Zhang, J. C. Gilhula, C. W. Abney and W. Lin, *J. Am. Chem. Soc.*, 2016, **138**, 3501-3509.
- M. Merckx, D. A. Kopp, M. H. Sazinsky, J. L. Blazyk, J. Müller and S. J. Lippard, *Angew. Chem. Int. Ed.*, 2001, **40**, 2782-2807.
- R. N. F. Thorneley and D. J. Lowe, *J. Biol. Inorg. Chem.*, 1996, **1**, 576-580.
- M. Delferro and T. J. Marks, *Chem. Rev.*, 2011, **111**, 2450-2485.
- M. Weiss and R. Peters, in *Cooperative Catalysis*, Wiley-VCH Verlag GmbH & Co. KGaA, 2015, DOI: 10.1002/9783527681020.ch8, pp. 227-262.
- H. Müller, W. Seidel and H. Görls, *J. Organomet. Chem.*, 1993, **445**, 133-136.
- C. Roukoss, J.-M. Basset, C. Copéret, C. Lucas and E. Kuntz, *Comptes Rendus Chimie*, 2008, **11**, 620-627.
- L. T. Zhuravlev, *Colloids Surf., A*, 2000, **173**, 1-38.
- NIST Computational Chemistry Comparison and Benchmark Database. NIST Standard Reference Database Number 101. Release 18, October 2016, Editor: Russell D. Johnson III. <http://cccbdb.nist.gov/>.
- E. Kose, A. Atac, M. Karabacak, P. B. Nagabalasubramanian, A. M. Asiri and S. Periandy, *Spectrochim. Acta, Part A*, 2013, **116**, 622-634.
- U. Das, G. Zhang, B. Hu, A. S. Hock, P. C. Redfern, J. T. Miller and L. A. Curtiss, *ACS Catal.*, 2015, **5**, 7177-7185.
- C. Copéret, D. P. Estes, K. Larmier and K. Searles, *Chem. Rev.*, 2016, **116**, 8463-8505.
- F. Bertini, N. Gorgas, B. Stöger, M. Peruzzini, L. F. Veiros, K. Kirchner and L. Gonsalvi, *ACS Catal.*, 2016, **6**, 2889-2893.
- R. Langer, Y. Diskin-Posner, G. Leituss, L. J. W. Shimon, Y. Ben-David and D. Milstein, *Angew. Chem. Int. Ed.*, 2011, **50**, 9948-9952.
- Y. Zhang, A. D. MacIntosh, J. L. Wong, E. A. Bielinski, P. G. Williard, B. Q. Mercado, N. Hazari and W. H. Bernskoetter, *Chem. Sci.*, 2015, **6**, 4291-4299.
- V. Kelsen, B. Wendt, S. Werkmeister, K. Junge, M. Beller and B. Chaudret, *Chem. Commun.*, 2013, **49**, 3416-3418.
- Note that the use of ethanol and sonication during TEM sample preparation could lead to re-dispersion of iron oxide nanoparticles.



81x41mm (150 x 150 DPI)